



## Grain statistics effect on deformation behavior in asymmetric rolling of pure copper foil by crystal plasticity finite element model

Shou-dong CHEN<sup>1</sup>, Xiang-hua LIU<sup>1</sup>, Li-zhong LIU<sup>2</sup>

1. State Key Laboratory of Rolling and Automation, Northeastern University, Shenyang 110819, China;

2. School of Materials and Metallurgy, Northeastern University, Shenyang 110819, China

Received 15 December 2014; accepted 12 May 2015

**Abstract:** The grain statistics effect was investigated through asymmetric rolling of pure copper foil by a realistic polycrystalline aggregates model and crystal plasticity element finite model. A polycrystalline aggregate model was generated and a crystal plasticity-based finite element model was developed for each grain and the specimen as a whole. The crystal plasticity model itself is rate dependent and accounts for local dissipative hardening effects and the original orientation of each grain was generated based on the orientation distribution function (ODF). The deformation behaviors, including inhomogeneous material flow, decrease of contact press and roll force with the increase of grain size for the constant size of specimens, were studied. It is revealed that when the specimens are composed of only a few grains across thickness, the grains with different sizes, shapes and orientations are unevenly distributed in the specimen and each grain plays a significant role in micro-scale plastic deformation and leads to inhomogeneous deformation and the scatter of experimental and simulation results. The slip system activity was examined and the predicted results are consistent with the surface layer model. The slip band is strictly influenced by the misorientation of neighbor grain with consideration of slip system activity. Furthermore, it is found that the decrease of roll force and the most active of slip system in surface grains are caused by the increase of free surface grain effect when the grain size is increased. The results of the physical experiment and simulation provide a basic understanding of micro-scaled plastic deformation behavior in asymmetric foil rolling.

**Key words:** foil rolling; grain heterogeneity; crystal plasticity; finite element; deformation behavior

### 1 Introduction

As the quick development in high technology field such as micro manufacturing, the needs to metal foil are increasing and the requirement to its quality is becoming strict. Micro-forming is a promising technology in manufacturing micro metal parts, because it offers many attractive virtues, such as higher production rates, better material integrity, less waste and lower manufacturing costs. However, when the part size is decreased to micro-scale, the mechanical behaviors of material change and the so-called size effect occurs. The size effect is characterized by grain size, specimen size, part feature size and surface topography. The design and fabrication of micro-parts by micro-forming cannot be conducted via leveraging on the knowledge of macro-forming process to micro-forming since the size effect is a barrier to this

knowledge transfer. In the development of foil rolling, miniaturization of the product and parts, where the size of some features may be similar to the grain size, and the heterogeneity of the deformation behavior attracts more and more attention. The anisotropic nature of crystal slip usually entails reorientation and subdivision phenomena during plastic strain of crystalline matter. This leads to spatial heterogeneity in terms of strain, stress, and crystal orientation. There has been increasing interest in the investigation on the plastic behaviors, mechanical properties and formability at microscale to design, fabricate and enhance the reliability of micro systems technology/micro-electrical-mechanical systems structures [1–7]. To analyze the quality of micro-parts, the material flow stress, anisotropy, ductility and formability in micro-scale need to be considered [8].

KIM and KU [9] proposed a new numerical approach to simulate the micro-strip rolling in which the

polycrystalline material was composed of regular hexagonal crystal grains and the grain unit was connected by the grain boundary unit accounting for shear deformation between neighbor grains. LAI et al [10] proposed a mixed stress–strain material model to describe the fine material forming progress. SHEN et al [11] established the relationship among the flow stress, billet dimension, and grain size based on crystal plasticity theory and surface layer model. MAHABUNPHACHAI and KOC [12] studied the grain size effect in hydraulic bulge test. They concluded that the interaction and interplay among grain size, feature size and specimen size affect the material deformation behavior significantly. CHAN et al [13] introduced a novel method based on the experimental results and composite model to analyze the effect of material microstructure characterizations on deformation behavior and scattering of material flow stress. However, those models of grain size effect are mainly focused on the change of grain boundary strengthening.

In recent years, the crystal plasticity finite element method (CPFEM) model has been widely developed to investigate the plastic deformation behavior of the single crystal and polycrystal experimentally and theoretically [14–16]. Micro radial compression tests were carried out on cylindrical specimens of pure copper polycrystal with different grain sizes by CHENG et al [17]. Experimental results indicated that phenomena of decreasing forming force, increasing scatter of forming force and more irregular surface topography occurred with the increase of grain size. LI et al [18] proposed an explicit polycrystal plasticity model to investigate the deformation mechanism of cold ring rolling in view of texture evolution. RAABE et al [19] simulated the micro-mechanical and macro-mechanical effects in grain scale polycrystal plasticity. The macroscopic plastic strain path is not completely altered by the crystallographic texture, but modulated following soft crystals and avoiding hard crystals. Grain-scale mechanisms are strongly superimposed by effects arising from the macroscopic profile of strain. KLUSEMANN et al [20] investigated the heterogeneity deformation of sheet metal with large grains via crystal plasticity finite element modeling. The focus in this initial study is on the deformation field development and evolution of the grain morphology during such loading.

The distribution of different grains with different orientations, sizes and shapes plays a significant role in the statistics size effect related phenomena such as inhomogeneous deformation behavior and the scattering of material properties when the formed part size is scaled down to micro-scale. As mentioned above, the modeling

and study considering these factors in foil rolling plastic deformation remain lacking. The aim of this work is to generate realistic gain morphology and to apply rate-dependent constitutive equations describing crystal plasticity in each grain, by means of a finite element code, to study the grain statistics effect on material plastic deformation behavior in the asymmetric rolling of pure foil.

## 2 Physical experiment

In the present work, the interaction effect between the specimen geometry size and grain size is mainly discussed. The effect is quantified by a ratio  $\varphi$  of the specimen size  $t$  to grain size  $d$  as follows:  $\varphi=t/d$ . Pure copper foils (T2) in the form of plates with dimensions of 30 mm (length)  $\times$  20 mm (width)  $\times$  0.1 mm (thickness) were used. The experiments of polycrystalline foil rolling with different grains across the thickness are presented. The annealing parameters and obtained grain size are shown in Table 1, and the microstructures after annealing are shown in Fig. 1. It can be seen that the grain size is increased, and the grains with different sizes are unevenly distributed in the foil and such unevenness is increased with the increase of the annealing temperature. Cold rolling was carried out on a multi-function rolling mill. The work rolls of 50 mm in diameter are independently driven by two motors. The upper roll carried out at constant rotational speed was taken to be 1.04 rad/s and the lower roll was able to use the variable velocity. The rolling speed ratio between the upper and lower rolls was set as 1.1. The thickness of the foil was reduced from 0.1 to 0.08 mm after one pass with 20% reduction. In each rolling process, the roll force was measured which will be compared with the simulation results.

**Table 1** Heat treatment parameters and obtained grain sizes

Annealing progress	Grain size/ $\mu\text{m}$	Number of grains over thickness
900 °C, 4 h	101	1
800 °C, 4 h	33	3



**Fig. 1** Microstructures of pure copper foil annealed under different conditions: (a) 900 °C, 4 h; (b) 800 °C, 4 h

### 3 Numerical simulation

#### 3.1 Crystal plasticity model

The crystal plasticity model adopted in this study is based on the rate-sensitivity and the details of crystal plasticity model can be seen in Ref. [21].

The total deformation gradient  $\mathbf{F}$  can be decomposed into a plastic part ( $\mathbf{F}^p$ ) and an elastic part ( $\mathbf{F}^e$ ) as

$$\mathbf{F} = \mathbf{F}^e \cdot \mathbf{F}^p \quad (1)$$

The velocity gradient  $\mathbf{L}$  is assumed to be decomposed into nonplastic ( $\mathbf{L}^e$ ) and plastic parts ( $\mathbf{L}^p$ ) as

$$\mathbf{L} = \mathbf{L}^e + \mathbf{L}^p \quad (2)$$

The plastic part of the velocity gradient  $\mathbf{L}^p$  is defined by the sum of the slip deformations of all slip systems as

$$\mathbf{L}^p = \sum_{\alpha=1}^N \dot{\gamma}^{(\alpha)} \mathbf{m}^{(\alpha)} \otimes \mathbf{n}^{(\alpha)} \quad (3)$$

where  $\mathbf{m}^{(\alpha)}$  and  $\mathbf{n}^{(\alpha)}$  are the slip plane normal and slip direction vectors, respectively;  $\dot{\gamma}^{(\alpha)}$  is the slip shear strain rate;  $N$  is the number of slip systems; the superscript  $\alpha$  denotes a specific slip system.

All geometrically possible slip systems with this model are activated by a power law relation between the shear strain rate  $\dot{\gamma}^{(\alpha)}$  and the resolved shear stress  $\tau^{(\alpha)}$ :

$$\begin{cases} \dot{\gamma}^{(\alpha)} = \dot{\gamma}_0^{(\alpha)} \operatorname{sgn}(\tau^{(\alpha)}) \left| \frac{\tau^{(\alpha)}}{\tau_c^{(\alpha)}} \right|^n, & \text{for } |\tau^{(\alpha)}| \geq \tau_c^{(\alpha)} \\ \dot{\gamma}^{(\alpha)} = 0, & \text{for } |\tau^{(\alpha)}| < \tau_c^{(\alpha)} \end{cases} \quad (4)$$

where  $\operatorname{sgn}(x)=1$  if  $x \geq 0$  and  $\operatorname{sgn}(x)=-1$  if  $x < 0$ ;  $\dot{\gamma}_0^{(\alpha)}$  is the reference value of the shear strain rate of the slip system  $\alpha$ , which is a constant for all slip systems;  $n$  denotes the rate-sensitive exponent and limit is  $0 \sim \infty$ ;  $\tau_c^{(\alpha)}$  is the critical resolved shear stress of the slip system  $\alpha$ .

BASSANI and WU hardening model [22] has been adopted to describe the flow and strain hardening that occurs on crystallographic slip systems:

$$\dot{\tau}_c^{(\alpha)} = \sum_{\beta=1}^N h_{\alpha\beta} \left| \dot{\gamma}^{(\beta)} \right| \quad (5)$$

$$h_{\alpha\alpha} = \left[ (h_0 - h_s) \sec h^2 \left( \frac{(h_0 - h_s) \gamma^{(\alpha)}}{\tau_1 - \tau_0} \right) + h_s \right] \cdot \left[ 1 + \sum_{\substack{\beta=1 \\ \beta \neq \alpha}}^N f_{\alpha\beta} \tanh \left( \frac{\gamma^{(\beta)}}{\gamma_0} \right) \right], \quad \text{for } \alpha = \beta \quad (6)$$

$$h_{\alpha\beta} = q h_{\alpha\alpha}, \quad \text{for } \alpha \neq \beta \quad (7)$$

where  $h_{\alpha\beta}$  is the hardening modulus including the self-hardening of each slip system ( $\alpha=\beta$ ) and latent hardening ( $\alpha \neq \beta$ );  $q$  is a latent hardening parameter;  $\gamma_0$  is the reference value of slip;  $\gamma$  is the shear strain;  $\tau_0$  is the initial critical resolved shear stress;  $\tau_1$  is the breakthrough stress where large plastic flow initiates;  $h_0$  is the hardening modulus just after the initial yield;  $h_s$  is the hardening modulus during easy slip and  $f_{\alpha\beta}$  represents the magnitude of the strength of a particular slip interaction between two slip systems  $\alpha$  and  $\beta$ . The factor  $f_{\alpha\beta}$  depends on the geometric relation between two slip systems. There are five constants for  $f_{\alpha\beta}$ , namely  $a_1$  (no junction),  $a_2$  (Hirth lock),  $a_3$  (coplanar junction),  $a_4$  (glissile junction) and  $a_5$  (sessile junction).  $h_{\alpha\alpha}$  consists of two components.

In the current work, the crystal plasticity constitutive model is implemented into ABAQUS/Standard (ABAQUS 6.13) by using UMAT. An implicit numerical integration procedure is adopted to solve the rate-dependent constitutive equations.

#### 3.2 Simulation model

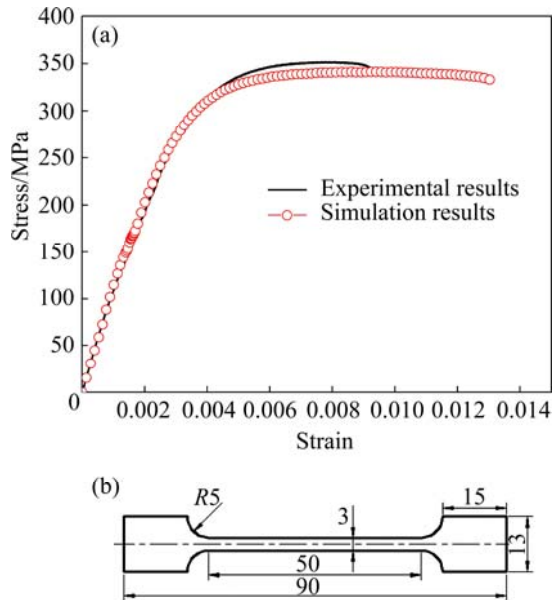
Slip is assumed to occur according to 12  $\{111\} \langle 110 \rangle$  systems corresponding to pure copper (FCC) and listed in Table 2. According to Refs. [22,23], the factors  $f_{\alpha\beta}$  for copper can be chosen as  $a_1=a_2=a_3=8$ ,  $a_4=15$ ,  $a_5=20$  and three elastic modules  $C_{11}=168400$  MPa,  $C_{12}=121400$  MPa and  $C_{44}=75400$  MPa. The unknown hardening parameters are calibrated by simultaneously fitting the stress-strain curve obtained from uniaxial tensile tests data on polycrystalline pure copper and finite element analysis. After trial and error test, one set of the model parameters are obtained and shown in Table 3. From the simulated and measured uniaxial tensile stress-strain curve (Fig. 2), the simulation result matches with experiment result very well.

**Table 2** Slip system considered in present study

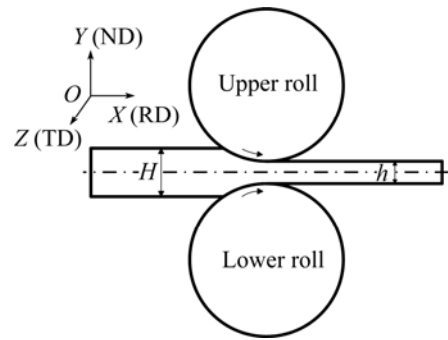
Slip system	Slip plane	Slip direction
a1	(111)	$[0\bar{1}1]$
a2		$[10\bar{1}]$
a3		$[\bar{1}10]$
b1	$(\bar{1}11)$	$[101]$
b2		$[110]$
b3		$[0\bar{1}1]$
c1	$(1\bar{1}1)$	$[011]$
c2		$[110]$
c3		$[10\bar{1}]$
d1	$(11\bar{1})$	$[011]$
d2		$[101]$
d3		$[\bar{1}10]$

**Table 3** Parameters in constitutive model

$n$	$\dot{\gamma}_0/\text{s}^{-1}$	$h_0/\text{MPa}$	$h_s/\text{MPa}$	$\tau/\text{MPa}$	$\tau_0/\text{MPa}$	$\gamma_0$
20	0.0001	90	1.5	1.3	1	0.001

**Fig. 2** Comparison of experimental and CPFEM simulated uniaxial tensile stress-strain curve (a) and dimensions of tensile specimen (b) (unit: mm)

A two-dimensional simulation of the cold foil rolling process was conducted by assuming plane strain condition. Figure 3 shows the schematic diagram of the two-dimensional rolling process and coordinate system, i.e.,  $X$  is the rolling direction (RD),  $Y$  is the normal direction (ND) and  $Z$  is the transverse direction (TD). Friction on the contact surface between roll and

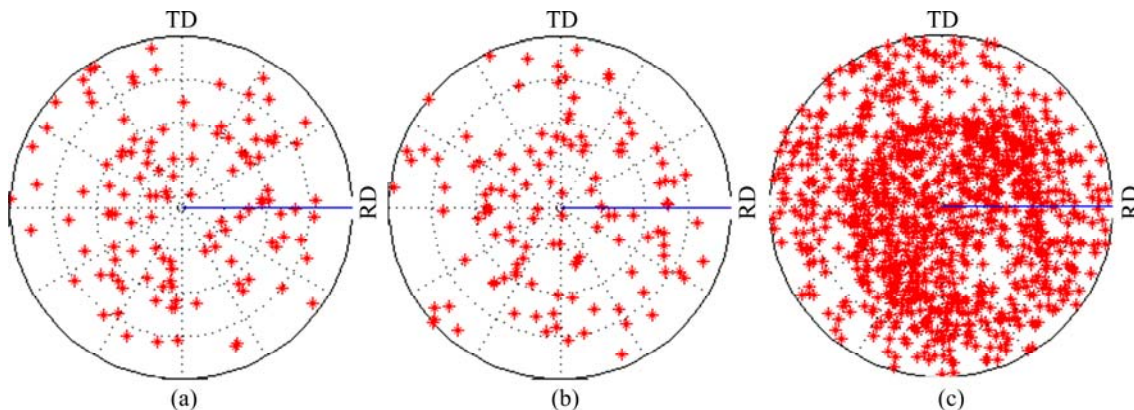
**Fig. 3** Schematic diagram of rolling progress and coordinate system

specimen is incorporated through the Coulomb's friction law with the coefficient of friction ( $\mu$ ). The condition of simulation cold foil rolling is the same as that of the rolling experiment and summarized in Table 4.

To account for the heterogeneity of polycrystalline structures possibly, a control model of virtual polycrystalline grain structures of Voronoï tessellation was used. The controlled Voronoï tessellation model is employed to generate virtual grain structures that are statistically equivalent to metallographic measurements in terms of grain size distribution. No certain texture for the grains in the foil after present annealing and so lattice orientations were randomly assigned in 3D to the model grains. In order to study the effect of the crystallographic orientation on the mechanical properties and reduce the influence of random factors as much as possible, for each geometry three grain orientation sets have been considered and three representative pole figures are shown in Fig. 4 which are generated using the Matlab's built-in function. It has to be noted that large number of

**Table 4** Initial cold foil rolling conditions for CPFEM simulation

$H/\text{mm}$	Length/mm	Upper roll rotational speed/( $\text{rad}\cdot\text{s}^{-1}$ )	Lower roll rotational speed/( $\text{rad}\cdot\text{s}^{-1}$ )	Reduction/%	$\mu$	Asymmetric speed coefficient
0.1	3	1.04	1.144	20	0.1	1.1

**Fig. 4** {1 1 1} pole figures: (a) Coarse grain model, orientation set 1; (b) Coarse grain model, orientation set 2; (c) Fine grain model, orientation set 3

grains result in a more uniform distribution of grain orientation than small number of grains. The mean grain size is kept constant, i.e., 101 and 33  $\mu\text{m}$  (equal to the experiment results). Two representative examples are shown in Fig. 5 and different colors represent different grain orientation. For the case of polycrystalline with coarse grains, there is only one grain across the thickness, 30 grains along the length, and the foil is divided by 4500 four-node plane strain elements. For the case of fine grain foils, there are three grains across the thickness, 90 grains along the length, and the foil is divided by 40500 CPE4R elements.

## 4 Results and discussion

Contour plots of accumulated slip in the coarse and fine grain model with different crystallographic orientation sets are shown in Fig. 6. It can be found that the accumulated slip in grains near two surfaces with

different crystallographic orientation sets is quite different from the coarse grain foil. However, the most grains have the relatively same accumulated shear strain for the fine grain foil. Shear band development in the microstructure is particularly illustrated in the fine grain foil. For the coarse grain foil, the maximum shear strain dispersedly appears in the areas which are the borders between grain boundary and surfaces of foil. For the fine grain foil, an apparent lower shear strain channel exists in the contour of accumulated slip distribution. Compared with the slip systems in the interior grain, the dislocation slip is constrained by the grain boundary, so the strain concentration of the slip systems around the boundary becomes larger at the grain boundary. The grain size and orientation have prior influence on the activity of plastic slip than strain gradient in foil rolling. The smaller the grain size is, the more homogeneous the plastic strain is produced.

Figure 7 shows FE contour plots of maximum

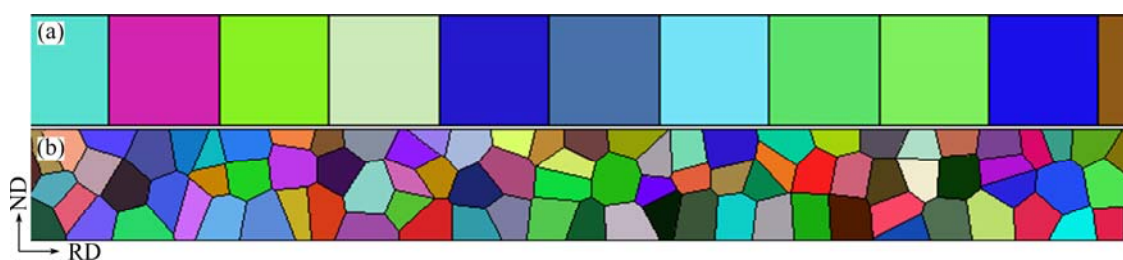


**Fig. 5** Example of grain structure and orientation: (a) Coarse grain; (b) Fine grain

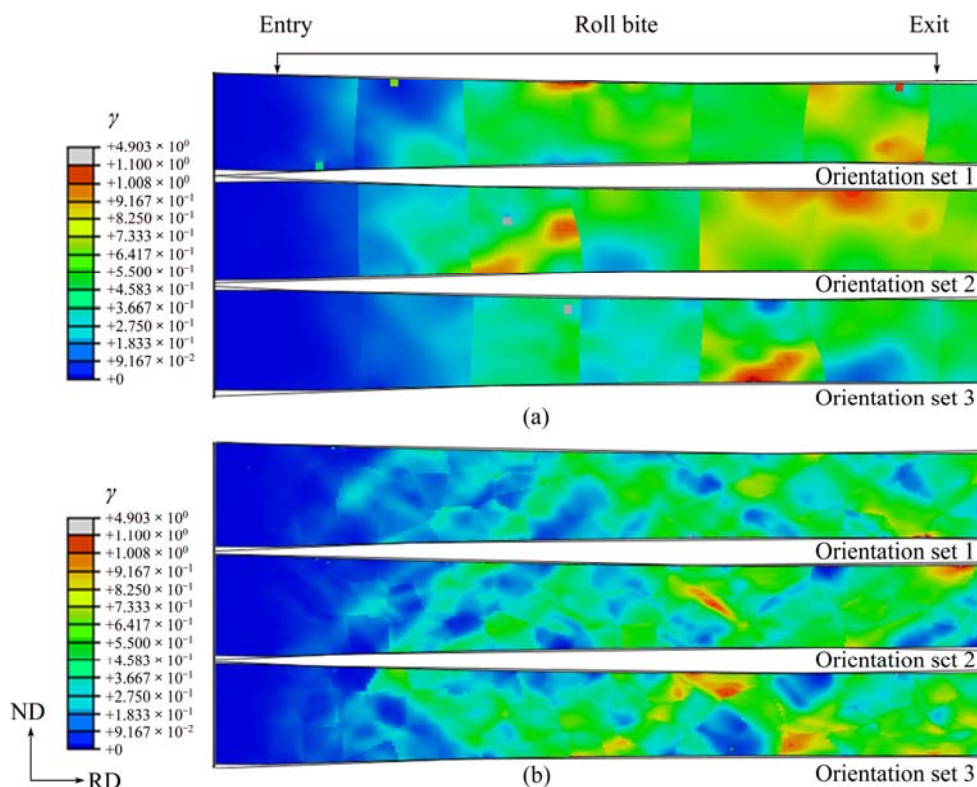


**Fig. 6** Contour plots of accumulated slip in plastic deformation zones during cold rolling with three crystallographic orientation sets: (a) Coarse grain; (b) Fine grain



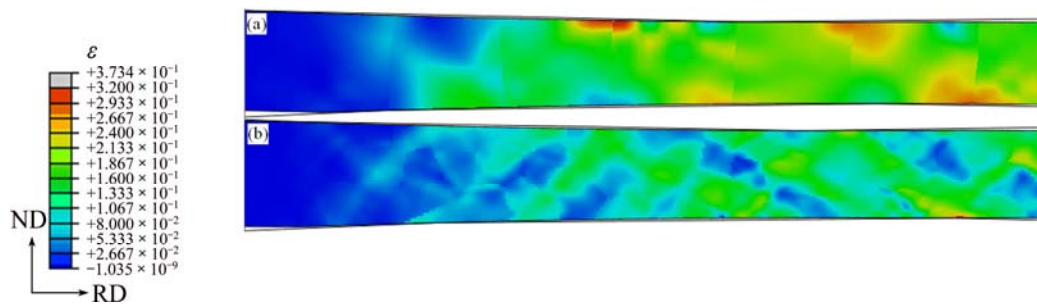


**Fig. 7** Distribution of max principal strain ( $\epsilon$ ) in rolling deformation zone with orientation set 1: (a) Coarse grain; (b) Fine grain

principal logarithmic strain in foil with the same thickness and length but different grain sizes. Generally, the strain distribution is inhomogeneous across the thickness and main plastic deformation zone spreads in the interior grain and at grain boundary. The strain gradient of some grains increases from the center of grain to the grain boundary, in contrast, the strain gradient of others decreases from the center of grain to the grain boundary. In the foil with one grain through the thickness, the deformation is quite inhomogeneous. However, in the foil with three grains through the thickness, the plastic deformation is far more regular. Shear bands are predicted to form in the center and surface of the fine grain foil, but not in the coarse grain foil.

Figure 8 shows the distributions of the frictional stress of coarse grain and fine grain foil with asymmetric speed coefficient of 1.1 in rolling deformation zone. From the entry of roll bite to the neutral point in symmetric rolling, the friction forces applied on the top and the bottom surfaces of foil are coincided with the flow of materials (backward slip zone). The friction force is opposite from the neutral point to the exit of the deformation zone (forward slip zone). Not only backward slip zone and forward slip zone, but also shear zone in which the friction force on the top and the bottom surfaces of the foil are against each other in asymmetric cold rolling. It can be seen that the frictional stress is sharply increased at some grain boundaries or intracrystalline, but others sharply decrease. As the number of the grains across the thickness section increases, the frictional stress in rolling bite also increases accordingly. For coarse grain foil, the distribution of frictional stress is severely scattered and dispersed, which is quite influenced by the individual grain orientation. From Fig. 8(b), it can be seen that the distribution of frictional stress of fine grain foil has a homogeneous and smooth pattern along the length of the rolling direction. Compared with the coarse grain foil, the length of shear zone for fine grain foil is longer. It is concluded that local friction between rolls and foil surface promotes an additional deformation, leading to

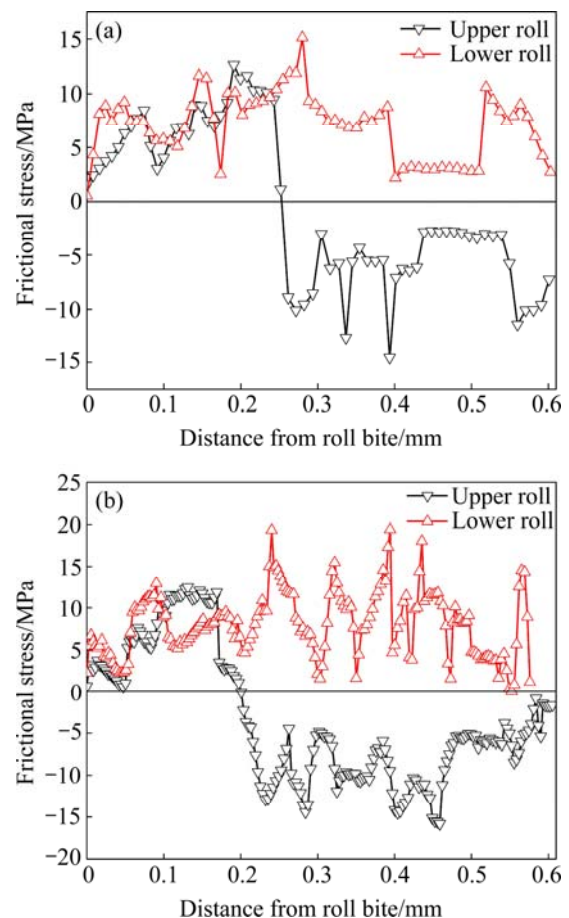


**Fig. 8** Distributions of frictional stress in deformation zone with orientation set 1: (a) Coarse grain; (b) Fine grain

contribution of plasticity strain and discrepancies in shear strain of grains.

Figure 9 presents the roll force per unit width with rolling time for coarse grain and fine grain foils. It is clear that the response of the coarse grain foils is much more heavily dependent on the crystallographic orientation set than that of the fine grain foils, especially in the latter stage of the rolling progress. Figure 9 highlights the influences of the grain size and orientation on the mechanical response for a constant specimen thickness, and presents the scatter of the roll force obtained for different original crystallographic

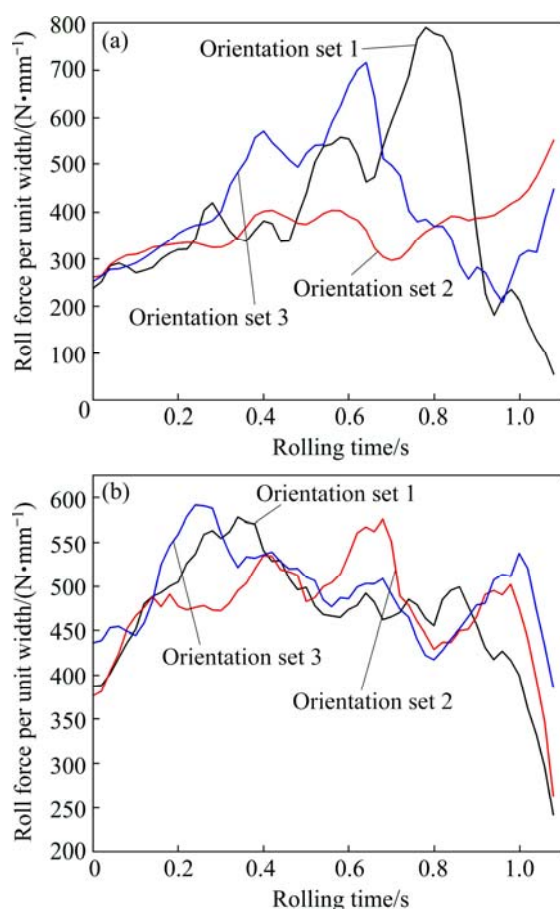


**Fig. 9** Distributions of roll force per unit width during rolling progress with three crystallographic orientation sets: (a) Coarse grain; (b) Fine grain

orientations. The microstructure dependence becomes manifest in the increase of the mutual differences between the calculated roll forces for coarse grain foil with constant thickness. In the coarse grain foil of only one grain over specimen thickness, the properties are increasingly dominated by individual grain. Large scatter can be expected when the original orientations are more dispersed. To establish a consistent metric for comparing the performance of the models in terms of grain statistics effect, the mean roll force per unit width was calculated and compared with the experimental results.

The computational and experimental results of the mean roll force per unit width are presented in Fig. 10 as a function of number of grains over foil thickness for all different original crystallographic orientations examined. The evident grain statistics effect illustrated by Fig. 10 is the reduction of roll force with increase of the grain size, which corresponds to experimental results. For the fine grain foil, there is no significant difference among different crystallographic orientation sets. There is a tendency for an increase in roll force scatter with decrease in number of grains over the thickness ( $\phi$ ). The scatter in the roll force per unit width can be related to

the grain structure. For the coarse grain foil, where there is only one grain in the thickness direction and the fraction of grain across thickness is large, the macroscopic behavior is heavily influenced by the properties of individual grain, and changing the crystallographic orientation can significantly alter the roll force response. But for fine grain foil, there exist 3 or 4 grains in the thickness direction, where individual grain influences are averaged out and it is more like macro-polycrystalline, and a more repeatable mechanical response is produced under variation of crystallographic orientation set.

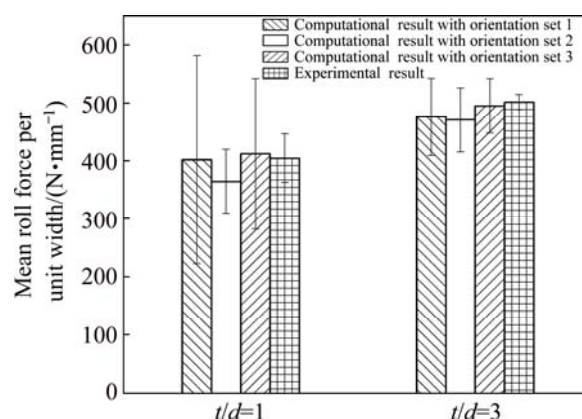


**Fig. 10** Plot of computational and experimental results of mean roll force per unit width with different initial crystallographic orientation sets (The error bars represent one standard deviation, with three crystallographic orientations simulated for each datum point)

The activity of the slip systems during asymmetric foil rolling was studied. In simulation, the crystal with its  $[1\ 0\ 0]$  axis coincident with the  $X$  direction,  $[0\ 0\ 1]$  and  $[0\ 1\ 0]$  axes coincident with the  $Y$  and  $Z$  directions, respectively, are shown in Fig. 3. According to the crystal plasticity constitutive laws described in Section 3.1, the activity of slip system  $\alpha$  is represented by  $\dot{\gamma}^{(\alpha)}$ . The illustration of  $(1\ 1\ 1)$  slip plane for FCC in rolling deformation is shown in Fig. 11. The slip system which

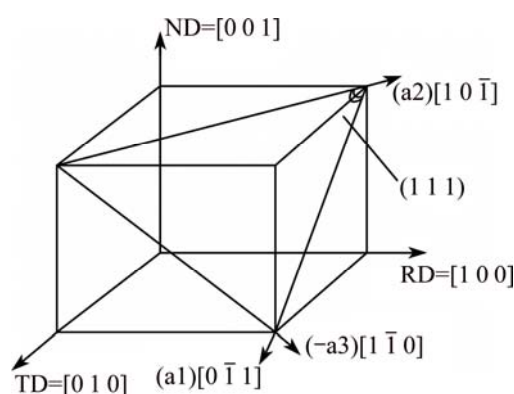


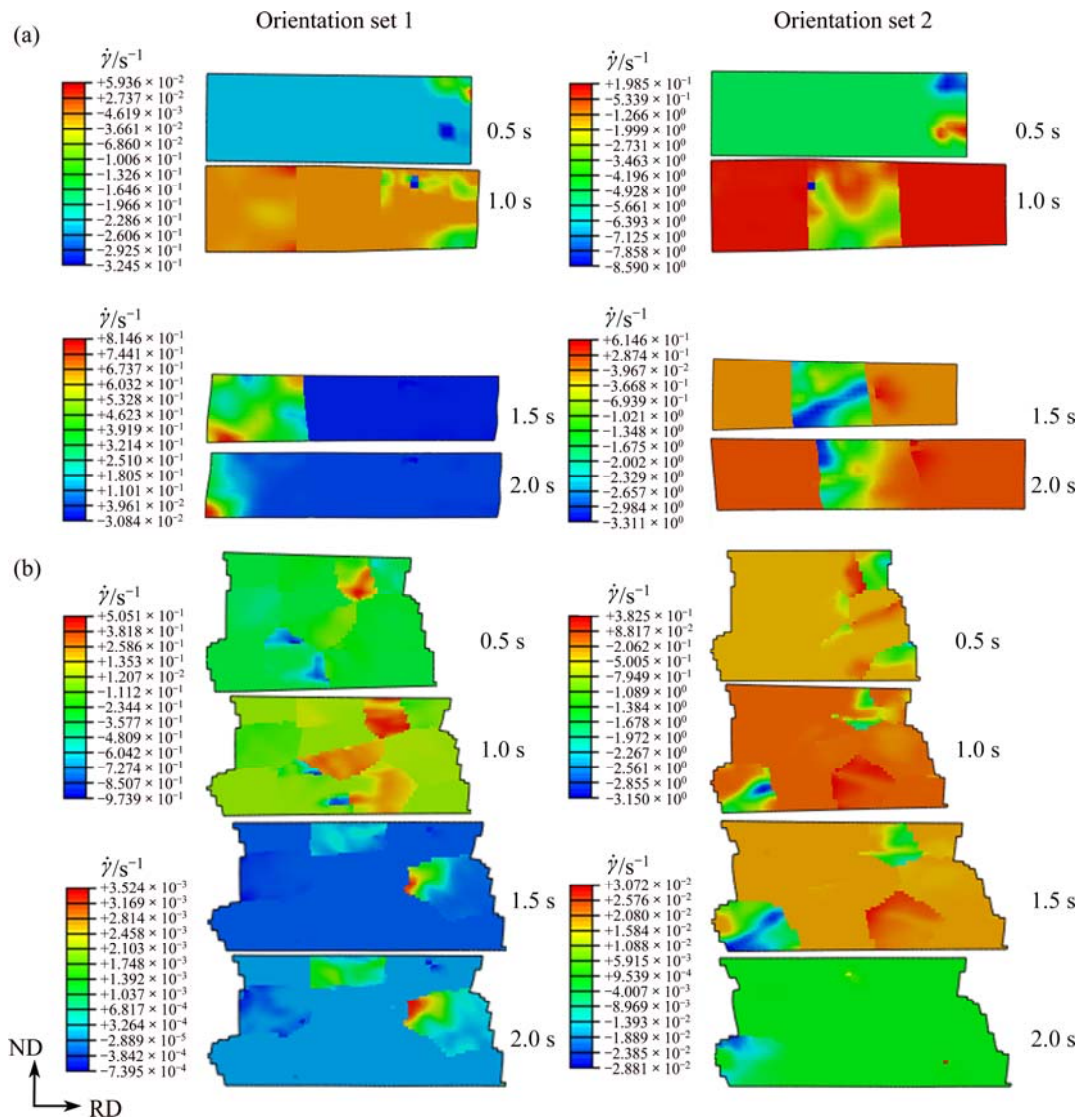
**Fig. 11** Illustration of  $(1\ 1\ 1)$  slip plane for initial rolling

might lead to deformation along the rolling direction should be easily activated due to the plane strain condition for rolling progress. Four principal slip systems satisfied the required deformation: (a3)  $(1\ 1\ 1)[\bar{1}\ 1\ 0]$ , (b2)  $(\bar{1}\ 1\ 1)[1\ 1\ 0]$ , (c2)  $(1\ \bar{1}\ 1)[1\ 1\ 0]$  and (d3)  $(1\ 1\ \bar{1})[\bar{1}\ 1\ 0]$ .

Figure 12 shows the evaluation of shear strain rate of slip system a3 of coarse and fine grain foils with two crystallographic orientation sets. It can be seen that crystallographic orientation has prior influence on the activity of slip system, which influences the activity of slip system in individual grain. It is obvious that the slip system a3 has the opposite shear strain rates on upper and lower surfaces for the coarse grain foil. The negative values indicated that the slip on this system should be along the  $[1\ \bar{1}\ 0]$  direction, which results in compression along ND and tension along RD. From Fig. 12, a significant slip of slip system a3 is produced on the upper and lower surfaces of the foil, for the both

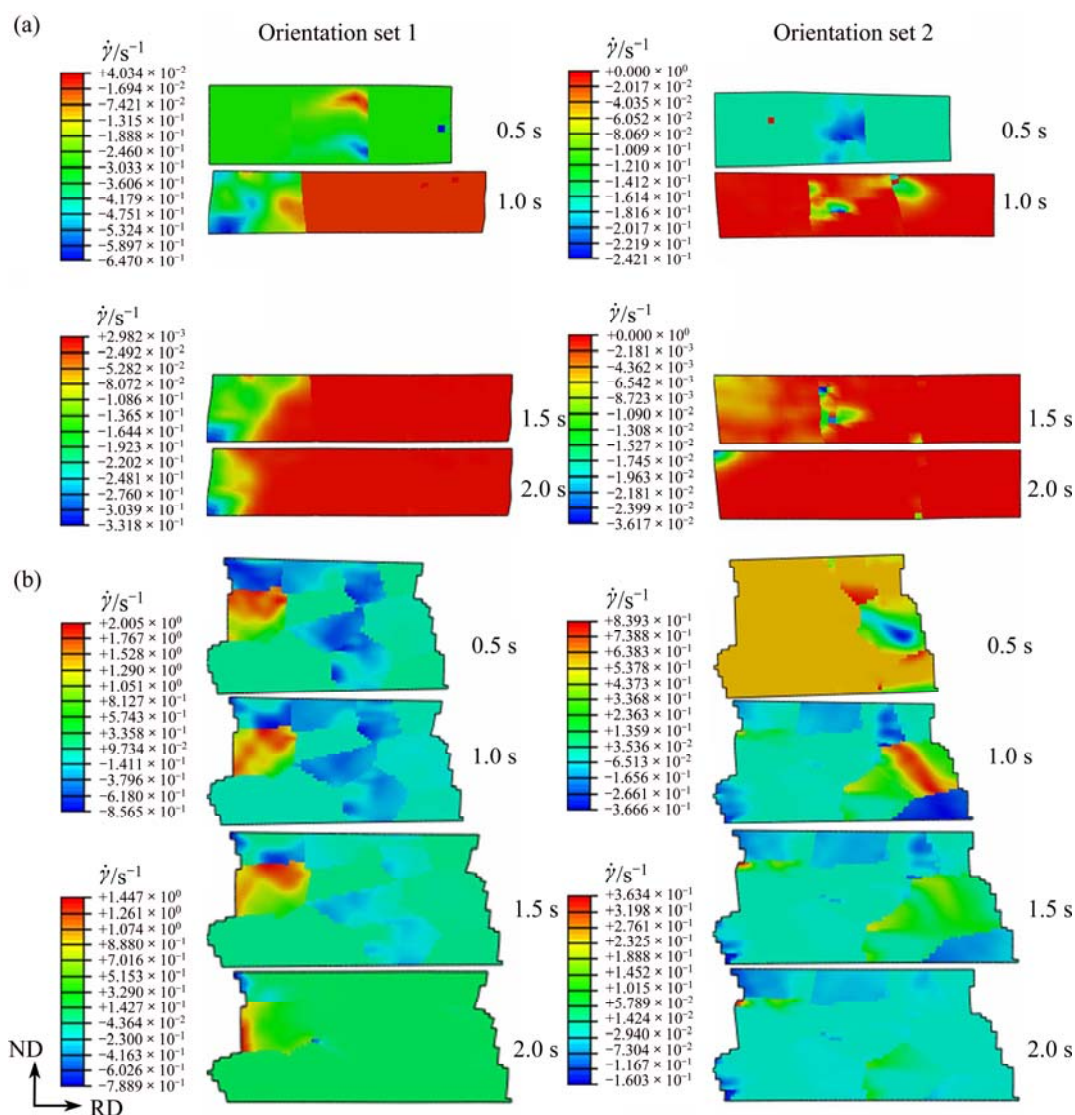
cases of original crystallographic orientation sets. Slip system a3 is more easily activated from the specimen surface and grain boundary than inter-grain or specimen center part. Compared with the fine grain foil, slip system a3 slips along the upper and lower surface direction for coarse grain foil and the slip band is formed, which crosses the thickness of the foil.

Figure 13 shows the evaluation of shear strain rate of slip system c2 of coarse and fine grain foils with two crystallographic orientation sets. The negative values indicated that the slip on c2 slip system should be along the  $[\bar{1}\ \bar{1}\ 0]$  direction, which results in compression along ND and tension along RD. For the orientation set 1, it can be found that a significant slip is produced in the vicinity of upper surface, for both cases of coarse grain and fine grain. For the orientation set 2, a significant slip is produced in the vicinity of grain boundary at the center of the foil, for both cases of coarse and fine grain. From Fig. 13, slip system c2 is slipped out of the foil from the



**Fig. 12** Simulated slip at four asymmetric rolling deformation states with two different crystallographic orientation sets for a3 slip system: (a) Coarse grain; (b) Fine grain





**Fig. 13** Simulated slip at four asymmetric rolling deformation states with two different crystallographic orientation sets for c2 slip system: (a) Coarse grain; (b) Fine grain

upper and lower surfaces during rolling progress in coarse foils, and only slipped out from the upper surface for the fine grain foil.

It can be seen that the slip systems are obstructed at grain boundary and slipped along the thickness direction. The results of activity of slip system are consistent with those of the free surface model predicted. From Figs. 12 and 13, it can be found that significant “positive–negative” slip patterns have been produced in individual grain, which indicates that the slip shear matrix bands are formed in inter-grain. After deformation, however, some grains’ lattice rotated significantly in the roll bite, showing the division of the initial grain into smaller sub-grains with new grain orientations.

The clear scatter of roll force that is predicted in Fig. 9 can be related to the grain structure of the foil. The deformation behavior of single grain is anisotropic. The deformation of polycrystalline metal is isotropic since

the grains with different sizes, shapes and orientations are evenly and randomly distributed within the foil. When the grain size is increased and the foil thickness is kept constant, there will be only a few grains over the thickness and the number of micro structural features is decreased. Individual grain plays a significant role in the overall material deformation behavior. Furthermore, different crystallographic orientations of neighboring grains lead to inhomogeneous deformation and the grains with different sizes, shapes and orientations result in the scatter of the measured material properties in the rolling progress.

The evident grain statistics effect illustrated by Fig. 10 is the reduction of the roll force with increasing the grain size and the thickness is kept constant, which correspond to the experimental results. This phenomenon can be explained by the increase of the relative contribution of surface grains and activity of the slip

system in those grains (Figs. 12 and 13). Coarse grain foil deformed easily than the fine grain foil because there are only a small number of grains across the thickness, and one grain in the thickness direction in the case of the coarse grain foil. When even one of these grains is in a favorable orientation for slip and when plastic strain localizes within it, it is relatively easy for forming a slip band to traverse the thickness direction with little constrain from surrounding grains, due to only one grain across the thickness. Contrasted with this situation, the fine grain foil where one grain only constitutes 1/3 of the thickness and if one of grains over thickness is favorably oriented for slip it will require higher macroscopic strain and stress level for the strain localization to develop into a macroscopic slip band across the thickness because the deformation of the grain is significantly constrained by the surrounding grains. With increasing the grain size, the grain boundary at grain interior is sharply decreased and the portion of free surface is greatly increased. The free surface did not represent a boundary comparable to a grain boundary, and thus the dislocation movement in surface grains was not restricted in the same way as in internal grains, yielding a less distinct hardening.

## 5 Conclusions

1) Due to different orientations, shapes and sizes of the grains located in the foil plane, the deformation is significantly inhomogeneous. The occurring spatial heterogeneity results in an increase of the scatter of the mechanical properties, producing local deformation. This phenomenon is more obvious for the coarse grain foils compared with the fine grains and leads to a decrease predictability of the mechanical response.

2) The development of the roll force during rolling progress depends on the number of the grains across the thickness direction. Both the contact press and roll force decrease with decreasing number of grains over the thickness of the foil. These effects can be explained by the increase of the effect of surface grain fraction.

3) The activity of slip system is no longer the same in grains because of different original crystallographic orientations and location. Slip systems are more easily activated and slipped in the surface grains than the inner grains for both the coarse grain and fine grain foils. The effect of surface grains on reduction of the roll force is illustrated by the active slip systems.

## References

- [1] FU M W, YANG B, CHAN W L. Experimental and simulation studies of micro blanking and deep drawing compound process using copper sheet [J]. *Journal of Materials Processing Technology*, 2013, 213(1): 101–110.
- [2] FU M W, CHAN W L. Geometry and grain size effects on the fracture behavior of sheet metal in micro-scale plastic deformation [J]. *Mater Design*, 2011, 32: 4738–4746.
- [3] WANG Chun-ju, GUO Bin, SHAN De-bin. Polycrystalline model for FE-simulation of micro forming processes [J]. *Transactions of Nonferrous Metals Society of China*, 2011, 21(6): 1362–1366.
- [4] CHAN W L, FU M W, LU J. The size effect on micro deformation behaviour in micro-scale plastic deformation [J]. *Mater Design*, 2011, 32: 198–206.
- [5] CHAN W L, FU M W. Experimental studies of plastic deformation behaviors in microbending process [J]. *Journal of Materials Processing Technology*, 2012, 212: 1501–1512.
- [6] CHAN W L, FU M W. Studies of the interactive effect of specimen and grain sizes on the plastic deformation behavior in microforming [J]. *International Journal of Advanced Manufacturing Technology*, 2012, 62: 989–1000.
- [7] CHENG Ming, ZHANG Shi-hong. Investigation of micro formability of bulk amorphous alloy in the supercooled liquid state based on fluid flow and finite element analysis [J]. *Journal of Materials Science & Technology*, 2009, 25(2): 277–280.
- [8] ENGEL U, ECKSTEIN R. Microforming-from basic research to its realization [J]. *Journal of Materials Processing Technology*, 2002, 125: 35–44.
- [9] KIM D J, KU T W. Finite element analysis of micro-rolling using grain and grain boundary elements [J]. *Journal of Materials Processing Technology*, 2002, 130–131: 456–461.
- [10] LAI X M, PENG L F, HU P, LAN S H, NI J. Material behavior modelling in micro/meso-scale forming process with considering size/scale effects [J]. *Computational Materials Science*, 2008, 43: 1003–1009.
- [11] SHEN Yu, YU Hu-ping, RUAN Xue-yu. Discussion and prediction on decreasing flow stress scale effect [J]. *Transactions of Nonferrous Metals Society of China*, 2006, 16(1): 132–136.
- [12] MAHABUNPHACHAI S, KOC M. Investigation of size effects on material behavior of thin sheet metals using hydraulic bulge testing at micro/meso-scales [J]. *International Journal of Machine Tools and Manufacture*, 2008, 48: 1014–1029.
- [13] CHAN W L, FU M W, LU J, LIU J G. Modeling of the grain size effect on the micro deformation behavior in micro-forming of pure copper [J]. *Materials Science and Engineering A*, 2010, 527(24): 6638–6648.
- [14] DIARD O, LECLERCQ S, ROUSSELIER G. Evaluation of finite element based analysis of 3D multicrystalline aggregates plasticity: Application to crystal plasticity model identification and the study of stress and strain fields near grain boundaries [J]. *International Journal of Plasticity*, 2005, 21: 691–722.
- [15] CHOI Y S, PARTHASARATHY T A. A crystal-plasticity finite element method study on effect of abnormally large grain on mesoscopic plasticity of polycrystal [J]. *Scripta Materialia*, 2012, 66: 56–59.
- [16] ROTERS F. Application of crystal plasticity FEM from single crystal to bulk polycrystal [J]. *Computational Materials Science*, 2005, 32: 509–517.
- [17] CHENG Li-dong, WANG Chuan-jie, WANG Chun-ju, GUO Bin, WANG Zhen-long. Size effects on plastic deformation behavior in micro radial compression of pure copper [J]. *Transactions of Nonferrous Metals Society of China*, 2013, 23(9): 2686–2691.
- [18] LI Hong-wei, FENG Lu, YANG He. Deformation mechanism of cold ring rolling in view of texture evolution predicted by a newly proposed polycrystal plasticity model [J]. *Transactions of Nonferrous Metals Society of China*, 2013, 23(12): 3729–3738.
- [19] RAABE D, SACHTLEBER M, ZHAO Z, ROTERS F, ZAEFFERER S. Micromechanical and macromechanical effects in grain scale polycrystal plasticity experimentation and simulation [J]. *Acta Materialia*, 2001, 49: 3433–3441.

- [20] KLUSEMANN B, SVENDSEN B, VEHOFF H. Investigation of the deformation behavior of Fe–3%Si sheet metal with large grains via crystal plasticity and finite-element modeling [J]. Computational Materials Science, 2012, 52: 25–32.
- [21] SI L Y, LU C, HUYNH N N, TIEU A K, LIU X H. Simulation of rolling behaviour of cubic oriented Al single crystal with crystal plasticity FEM [J]. Journal of Materials Processing Technology, 2008, 201: 79–84.
- [22] BASSANI J L, WU T Y. Latent hardening in single crystals II. Analytical characterization and predictions [J]. Proceedings of the Royal Society A, 1991, 435: 21–41.
- [23] HUANG Y G. Division of engineering and applied science [D]. USA: Harvard University, 1991.

## 基于晶体塑性有限元模型的 异步轧制纯铜箔变形行为晶粒统计效应

陈守东<sup>1</sup>, 刘相华<sup>1</sup>, 刘立忠<sup>2</sup>

1. 东北大学 轧制技术及连轧自动化国家重点实验室, 沈阳 110819;

2. 东北大学 材料与冶金学院, 沈阳 110819

**摘 要:** 采用一种真实的多晶集合体模型和晶体塑性有限元模型, 研究异步轧制纯铜箔塑性变形晶粒统计效应。考虑局部硬化耗散作用, 根据取向分布函数在取向空间中的分布规律将晶体取向分配给各个晶粒的单元积分点, 建立弹塑性大变形条件下的相关多晶体塑性模型, 并将其引入隐式有限元法。对非均匀材料流动、铜箔厚度一定时接触压力和轧制力随晶粒尺寸增加而降低的变形行为进行研究。结果表明, 在箔材厚度方向上只有少数几个晶粒时, 晶粒尺寸、形貌和取向不再均匀分布于箔材中, 材料的变形行为主要受到单个晶粒变形行为的影响, 从而导致非均匀变形及模拟和实验结果更加离散。研究变形过程中滑移系的启动过程, 晶粒取向对滑移系的启动和滑移带的形成具有重要影响, 预测结果与表面层模型一致。随着晶粒尺寸的增加, 表层晶粒效应增大, 更加有利于降低轧制力和激活表层晶粒内滑移系的开动。通过箔材轧制实验和模拟, 可以更加深入地理解异步轧制极薄带微塑性变形的机理。

**关键词:** 极薄带轧制; 晶粒各向异性; 晶体塑性; 有限元; 变形行为

(Edited by Xiang-qun LI)